5 Understanding The Hubbard Model With Simple Calculations

Richard T. Scalettar
University of California Davis
Department of Physics and Astronomy, One Shields Ave., Davis, CA 95616

Contents

1 Introduction

The Hubbard Hamiltonian,

$$\hat{\mathcal{H}} = -t \sum_{\langle jl \rangle \sigma} \left(\hat{c}^\dagger_{l\sigma} \hat{c}_{j\,\sigma} + \hat{c}^\dagger_{j\,\sigma} \hat{c}_{l\sigma} \right) + U \sum_l \hat{n}_{l\uparrow} \hat{n}_{l\downarrow} - \mu \sum_l \hat{n}_{l\sigma} \tag{1}$$

describes the 'hopping' of two species of fermions, spin $\sigma =\uparrow, \downarrow$, on neighboring sites $\langle lj \rangle$ of a lattice, and interacting, when on the same site l, with an energy U. Here $\hat{n}_{l\sigma} = \hat{c}^\dagger_{l\sigma} \hat{c}_{l\sigma}$ is the fermion number operator and μ is the chemical potential. I am going to assume we are all familiar with the basic properties of fermion creation and destruction operators $\hat{c}^\dagger_{l\sigma}$ and $\hat{c}_{l\sigma}$, including, for example, their anticommutation relations, $\left\{ \hat{c}^\dagger_{l\sigma}, \hat{c}_{j\sigma} \right\} = \delta_{jl} \delta_{\sigma\sigma'}$ and $\left\{ \hat{c}^\dagger_{l\sigma}, \hat{c}^\dagger_{j\sigma} \right\} = 0$.

A discussion of the Hubbard Hamiltonian is a truly immense undertaking. From a temporal point of view it encompasses a six decade history spanning the work of Hubbard, Anderson and Mott in the 1960's through a host of materials to which it has been applied: transition metal oxides, heavy fermions, cuprate superconductors, etc [1]. Indeed, in the last 15 years a major focus of the Atomic and Molecular (AMO) community has been on realizing and characterizing the Hubbard model in systems of ultracold atoms [2, 3]. Attempts to solve the Hubbard model computationally have driven a rich set of stories in inhomogeneous Hartree-Fock (stripe formation) [4], Quantum Monte Carlo (QMC) [5] (including the famous 'sign problem'), density matrix renormalization group (DMRG) methods [6], and machine learning [7]. A recent review summarizes the breadth of these developments, applications and connections [8].

From a pedagogical point of view, the danger of a lecture (or even several lectures) on the Hubbard model is the temptation to do too much. The audience is then left with a sense of the breadth and excitement of the field, but not with a concrete ability to '*do something*'.

The objectives of this lecture are to provide some specific calculations which shed light on the basic physics of the Hubbard model. We will begin with the non-interacting limit, i.e. obtaining the 'band structure' of the Hubbard model. We will emphasize that this already allows contact with some fascinating phenomena- localization by disorder, Fermi surface nesting and a divergence of the density of states linked to magnetism and superconductivity, and flat bands in which the electron energy is independent of momentum.

We will also describe two very interesting aspects of the non-interacting case. First, we will consider what happens when the motion of fermions to the left and to the right is unbalanced (the 'Hatano-Nelson' model). In this case the Hamiltonian is non-Hermitian (!!). Second, we will relate a special choice of hoppings which can realize the surprising phenomenon of 'perfect quantum state transfer'.

After discussing the $U = 0$ limit, and these two interesting situation, we will examine the opposite situation when $t = 0$, or, more generally, the strong coupling case $U >> t$. This

will give us insight into a fundamental feature of Hubbard model, the 'Mott plateau', where the density gets frozen at half-filling for an extended range of chemical potential.

The final objective is to describe the consequences of a set of canonical transformations which can be performed on the Hubbard model. We will see these allow us to discern surprising and not immediately intuitive physics in some parameter regimes from the more evident physics in others. Our first illustration will be on the by now well-known connections between magnetism in the repulsive Hubbard models and s-wave superconductivy and charge density wave formation in the attractive Hubbard model. We will then turn to a recent discovery of a tranformation which leads to a rigorous demonstration of a model exhibiting pair density wave formation, a phase of matter which has proven elusing to achieve both experimentally and theoretically.

2 A classical mechanics prelude

Let's begin with a familiar, but seemingly completely unrelated problem, which will prove to have close mathematical analogies with the non-interacting Hubbard model. Consider a one-dimensional array of N uniform masses m connected to their neighbors by uniform springs γ. Newton's equations of motion are,

$$m\frac{d^2x_l}{dt^2} = -\gamma\big(\,x_l - x_{l+1}\,\big) - \gamma\big(\,x_l - x_{l-1}\,\big) \tag{2}$$

where $x_l(t)$ is the displacement from equilibrium of mass l at time t. We solve this problem with the *ansatz* $x_l(t) = a_l\, e^{i\omega t}$ which reduces the N coupled differential equations to N coupled algebraic equations for the amplitudes a_l. After cancelling the common factor of $a_0\, e^{i\omega t}$ from all the terms,

$$m\omega^2\, a_l = \gamma\big(\,a_l - a_{l+1}\,\big) + \gamma\big(\,a_l - a_{l-1}\,\big) \tag{3}$$

These equations are solved by introducing normal mode coordinates

$$a_l = e^{-ikl}a_0, \tag{4}$$

yielding the normal mode frequencies

$$\omega^2(k) = 2\gamma\big(1 - \cos(k)\big) \tag{5}$$

where we have now used notation emphasizing the frequency depends on the 'momentum' k. (We will come back shortly to why calling k the momentum makes sense.)

Eq. 5 is an embarassment of riches. From a collection of N linear equations (Eqs. 3) we have an *infinite* set of solutions labeled by the continuous parameter k. Something is wrong, and it's because we did not treat the boundary conditions carefully. Equations 3 are only true for the masses which have both left and right neighbors, $l = 2, 3, \cdots N$-1. The two masses at the end have only a single neighbor if we adopt 'open boundary conditions' (obc). Here instead we

use 'periodic boundary conditions' (pbc), and link oscillator $l = 1$ to oscillator $l = N$ with an extra spring of potential energy $\frac{1}{2}\gamma(x_1 - x_N)^2$. Then Eqs. 3 apply to *all* x_l, if we demand that $x_0 \equiv x_N$ and $x_1 \equiv x_{N+1}$.

This solves our problem of too many solutions, since it quantizes the previously unrestricted allowed values of momentum by requiring $e^{ikN} = 1$ or, in other words, $k \in \frac{2\pi}{N}\{1, 2, \cdots, N\}$. Because cosine is periodic, it is equivalent to set $k = \frac{2\pi}{N}\{-\frac{N}{2} + 1, -\frac{N}{2} + 2 \cdots \frac{N}{2}\}$. which has the advantage of making k more symmetric about $k = 0$.

It is useful to consider two special cases. When $k = 0$ all masses have identical displacements $a_l = a_0$. The entire chain is shifted rigidly and $\omega(k) = 0$. This is an example of a zero frequency 'Goldstone mode' associated with the translational invariance of our mass-spring system. (Because only inter-mass springs are present, there is no potential tying any mass to a particular location in space. As a sequence the energy is invariant under a simultaneous translation of all the masses. Put another way, the choice of origin is irrelevant.) On the other hand, when $k = \pi$ the masses alternate $a_l = a_0\, e^{i\pi l} = a_0(-1)^l$. This results in the largest normal mode frequency (energy), $\omega^2 = \frac{4k}{m}$. (There is an interesting analogy with quantum mechanics here. If you sketch a_l versus l for this highest energy mode, you see there is a node between every mass. a_l wiggles as fast as possible. Similarly, in quantum mechanics we know that wiggly wave functions are associated with high kinetic energy.)

One can also solve the obc case. The 'dispersion relation' giving the functional form for $\omega(k)$ is unchanged, but the N allowed momenta are shifted slightly to $k \in \frac{2\pi}{N+1}\{0, 1, 2, \cdots N\text{-}1\}$. The pbc case is a bit more simple, so we use it here. Besides simplicity, it is also the case that properties measured in finite length N chains with pbc are closer to the thermodynamic limit $N = \infty$ than obc. (Specifically, finite size corrections often go as $\frac{1}{N^2}$ with pbc and $\frac{1}{N}$ with obc.)

A closing observation is that this solution of coupled oscillators all goes horribly wrong in the presence of anharmonicity. Indeed, even a single anharmonic oscillator, the solution of $F = ma$ with $V(x) = \frac{1}{2}kx^2 + \frac{1}{4}ux^4$ is intractable. As we shall see below, the presence of quartic terms ux^4 in the fermion creation and destruction operators are precisely what makes the Hubbard model impossible to solve for U non-zero.

That's a long time spent on classical mechanics! But we will see now that the exact same mathematics underlies the solution of the non-interacting Hubbard model.

3 The Hubbard Model at $U = 0$

The 1D Case (linear chain)

Let's write down the non-interacting ($U = 0$) Hubbard model for a 1D chain.

$$\hat{\mathcal{H}} = -t \sum_l \left(\hat{c}^\dagger_{l\sigma} \hat{c}_{l+1\,\sigma} + \hat{c}^\dagger_{l+1\,\sigma} \hat{c}_{l\sigma} \right) - \mu \sum_l \hat{c}^\dagger_{l\sigma} \hat{c}_{l\sigma} \tag{6}$$

Because we will not have any interactions for this Section, we will suppress the spin index σ on the fermionic operators. That is, since U is the only thing that connects fermions with $\sigma =\uparrow$ to fermions with $\sigma =\downarrow$, when $U = 0$ we can just solve each spin sector independently.

Now just as we defined normal mode coordinates for the positions of our masses we can also here define linear combinations of

$$\hat{c}_k^\dagger \equiv \frac{1}{\sqrt{N}} \sum_l e^{ikl} \hat{c}_l^\dagger \tag{7}$$

and its inverse,

$$\hat{c}_l^\dagger \equiv \frac{1}{\sqrt{N}} \sum_l e^{-ikl} \hat{c}_k^\dagger. \tag{8}$$

Note the reemblance between Eqs. 7 and 4. The fermion creation operator transformation is, however, a little more subtle than the classical mechanics case, because we must be sure that our new operators $\hat{c}_k$ obey the same fermionic anti-commutation relations as the originals. It is easy to prove this from the identities

$$\frac{1}{N} \sum_l e^{i(k-k')l} = \delta_{kk'} \tag{9}$$

and

$$\frac{1}{N} \sum_k e^{i(l-l')k} = \delta_{ll'} \tag{10}$$

which hold for the discrete allowed momenta $k, k' \in \frac{2\pi}{N}\{-\frac{N}{2}+1, -\frac{N}{2}+2 \cdots \frac{N}{2}\}$. Equations 9 and 10 are the discrete analogs of the familiar orthogonality relations used in Fourier transforms.

Plugging the transformation Eq. 8 into the Hamiltonian, Eq. 6, and making use of Eqs. 9 and 10 yields

$$\hat{\mathcal{H}} = \sum_k \big(E_k - \mu \big) \hat{c}_k^\dagger \hat{c}_k \tag{11}$$

where

$$E(k) = -2t \cos(k) \tag{12}$$

The similarity between the right-hand sides of Eqs. 5 and 12 should be evident, from the appearance of $\cos(k)$ to $2\gamma \leftrightarrow -\mu$. The energy levels of the 1D Hubbard chain range from $-2t \leq E(k) \leq +2t$. One refers to this range as the 'bandwidth' $W = 4t$.

It is interesting to think about the physics of the structure on Eq. 11. The Hamiltonian does not 'mix' different values of momentum k. When an electron of momentum k is destroyed, all that can happen is that an electron with the *same* momentum be created. This is the analog of the

classical mechanical principal that normal modes do not mix: A system set into oscillation in a particular normal mode remains in that mode forever, and none of the others ever get excited.

Concerning the left-hand sides, one can wonder why the frequency/energy appears linearly in Eq. 12 in the quantum problem, whereas it was quadratic in the coupled oscillator calculation Eq. 5. The answer, of course, lies in the fact that Newton's equations involve $\frac{d^2}{dt^2}$, whereas the Schroedinger equation involves only $\frac{\partial}{\partial t}$.

We have exploited the translation invariances of the oscillator system and the Hubbard Hamiltonian to guess (make an *ansatz*) to extract the normal modes/band structure. In the absence of such symmetries the problem bcomes one of diagonalizing a matrix.

Put another way, we can write the Hubbard Hamiltonian as

$$\hat{\mathcal{H}} = \begin{pmatrix} \hat{c}_1^\dagger & \hat{c}_2^\dagger & \hat{c}_3^\dagger & \hat{c}_4^\dagger & \hat{c}_5^\dagger & \cdots \end{pmatrix} \begin{pmatrix} -\mu & -t & 0 & 0 & 0 & \cdots \\ -t & -\mu & -t & 0 & 0 & \cdots \\ 0 & -t & -\mu & -t & 0 & \cdots \\ 0 & 0 & -t & -\mu & -t & \cdots \\ 0 & 0 & 0 & -t & -\mu & \cdots \\ \vdots & \vdots & \vdots & \vdots & \vdots & \ddots \end{pmatrix} \begin{pmatrix} \hat{c}_1 \\ \hat{c}_2 \\ \hat{c}_3 \\ \hat{c}_4 \\ \hat{c}_5 \\ \vdots \end{pmatrix} \tag{13}$$

We happen to know (if we have some experience with tri-diagonal matrices) the eigenvalues and eigenvectors of the matrix in Eq. 13. The eigenvalues are just the $E(k)$ in Eq. 12, and the matrix of eigenvectors has entries $\Psi_{kl} = e^{ikl}$. I have used the notation Ψ deliberately, because these eigenvectors are quite literally the familiar plane-wave solutions of the free particle Schroedinger equation (on a discrete lattice). This justifies our referring to k as the momentum.

If we had not known this similarity transformation, we would have proceeded by diagonalizing the matrix by calling an appropriate BLAS/LAPACK routine. While we should (and have) avoid solving the eigenproblem numerically, it is worth emphasizing it is not at all a big deal. We shall see the utility of this way of thinking in terms of matrix diagonalization when we discuss localized modes in the non-interacting Hubbard model.

Equation 12 gives the energy of a single electron, that is the energy of the state $|k\rangle = c_k^\dagger|\text{vac}\rangle$. It remains to discuss the computation of the energy with M electrons. The prescription is simple: if several electrons are present, the state $|\, k_1\, k_2\, \cdots k_M\, \rangle = c_{k_1}^\dagger c_{k_2}^\dagger \cdots c_{k_M}^\dagger|\text{vac}\rangle$ has energy $E(k_1) + E(k_2) + \cdots E(k_M)$. Of course the Pauli principle forbids any of the k_i from being the same.

If we are interested in the ground state of M electrons, we fill up (occupy) the states of lowest energy. The 'Fermi Energy' is the highest energy that is occupied for M particles. The seemingly mysterious choice of the minus sign in front of the hopping parameter t makes momentum $k = 0$ have the lowest energy, with a Fermi surface enclosing it.

Once we have the dispersion relation in hand, a very important quantity is the density of states $A(\omega)$. In words, $A(\omega)d\omega$ gives the number of $E(k)$ values which like between ω and $\omega + d\omega$.

Formally,

$$A(\omega) \equiv \frac{1}{N}\sum_k \delta\big(\,\omega - E(k)\,\big) \tag{14}$$

We can easily get $A(\omega)$ in the limit $N \to \infty$ where the k values become continuous

$$A(\omega) = \frac{1}{2\pi}\int_{-\pi}^{+\pi} \delta\big(\,\omega + 2t\cos(k)\,\big) = \frac{1}{\omega^2 - 4t^2} \tag{15}$$

We have used the presciption $\frac{1}{N}\sum_k \to \frac{1}{2\pi}\int dk$ in going from a sum over discrete values separated by $\frac{2\pi}{N}$ to an integral.

The 2D Square Lattice

On a 2D square lattice, the noninteracting Hubbard Hamiltonian is

$$\hat{\mathcal{H}} = -t\sum_{l_x,l_y}\big(\,\hat{c}^\dagger_{l_x,l_y}\hat{c}_{l_x+1,l_y} + \hat{c}^\dagger_{l_x+1,l_y}\hat{c}_{l_x,l_y} + \hat{c}^\dagger_{l_x,l_y}\hat{c}_{l_x,l_y-1} + \hat{c}^\dagger_{l_x,l_y-1}\hat{c}_{lx,l_y}\,\big) - \mu\sum_{l_x l_y}\hat{c}^\dagger_{l_x,l_y}\hat{c}_{l_x,l_y} \tag{16}$$

Although it is useful to work through the algebra for practice, the result is pretty reasonable, and we will just quote it. The process is just to redo the steps of Sec. 2.1 with $l \to l_x, l_y$. The result is

$$\hat{\mathcal{H}} = \sum_{k_x,k_y}\big(\,E(k_x,k_y) - \mu\,\big)\hat{c}^\dagger_{k_x,k_y}\hat{c}_{k_x,k_y} \tag{17}$$

where

$$E(k_x,k_y) = -2t\cos(k_x) - 2t\cos(k_y) \tag{18}$$

gives the energy of an electron of momentum k_x, k_y. The energy levels of the Hubbard model on a square lattice range from $-4t \le E(k_x,k_y) \le +4t$. The bandwidth $W = 8t$.

For many fermions, we again get the energy by just summing up the single particle levels out to a maximum Fermi Energy. However, in $d > 1$ one can ask for the shape of the contour of the boundary between the occupied and unoccupied k_x, k_y. This is referred to as the 'Fermi surface' (FS). For small k_x, k_y we can expand the cosines in Eq. 18 and

$$E(k_x,k_y) \sim -4t + t\,(\,k_x^2 + k_y^2\,) \tag{19}$$

and the FS is a circle about $(k_x,k_y) = (0,0)$. Thinking in analogy with $E(k) = \hbar^2(k_x^2+k_y^2)/2m$ we see that the effective mass of the fermions $m \sim 1/t$.

In general $E(k)$ is not quadratic and the FS does not have a circular topology (sphere in three dimensions). Indeed, the FS's for different fillings (number of fermions) are shown in the left panel of Fig. 1. An interesting feature of the dispersion relation of Eq. 18 is 'perfect nesting'. As seen in the right panel of Fig. 1, when the interior of the FS encompasses half of the allowed

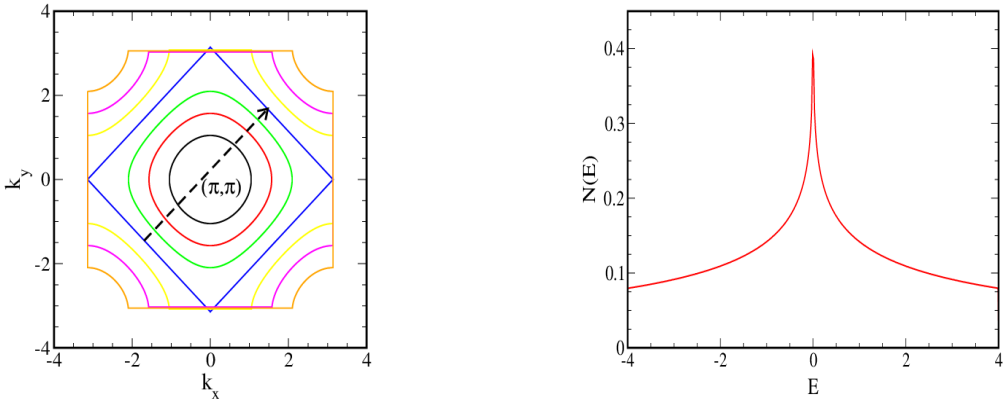

Fig. 1: *Left: The Fermi surfaces of the Hubbard model an a square lattice with nearest neighbor hopping. Right: The density of states of the Hubbard model an a square lattice with nearest neighbor hopping. There is a divergence ('van Hove singularity') of $N(\omega)$ at $\omega = 0$ (half filling).*

momenta $-\pi < k_x, k_y < +\pi$ (and hence the lattice is half-filled), the FS is a 'rotated square' and has the feature that a single wave-vector $(k_x, k_y) = (\pi, \pi)$ connects many points on the FS. This phenomenon is referred to as 'nesting'.

The second is a 'van Hove singularity' in the density of states.

It turns out that both of these properties make the square lattice Hubbard model particularly prone to assuming ordered phases when the interaction U is turned on. The rough reason appeals to your knowledge of second order perturbation theory, where you know the effect of a perturbation $\hat{V}$ is to shift the energy E_n of eigenstate $|n\rangle$ by $E^{(2)}{}_n = \sum_{m \neq n} \frac{|\langle n|\hat{V}|m\rangle|^2}{E_n - E_m}$. If there are many states with $E_m = E_n$ the effect of $\hat{V}$ will be very large and this is precisely what happens with perfect nesting.
are materials like the cuprate superconductors for which the square lattice is appropriate.

The Lieb Lattice and "Flat Bands"

An interesting feature of the square lattice is that its sites can be divided into two sublattices (red and green in the left panel of Fig. 2) such the near neighbors of red sites are always green and the near neighbors of green sites are always red. Such a geometry is said to be 'bipartite', and this property has deep implications for the physics.

The honeycomb lattice describing the positions of the carbon atoms in a sheet of graphene is also bipartite. In both the square and honeycomb cases, the numbers of red and green sites are identical. We will next consider the Hubbard model on a Lieb lattice, shown in Fig. 2.

Although we blitzed through going from a 1D chain to a 2D square lattice, it is worth being a bit more careful with this one, because going to momentum space does not quite complete the process of diagonalization.

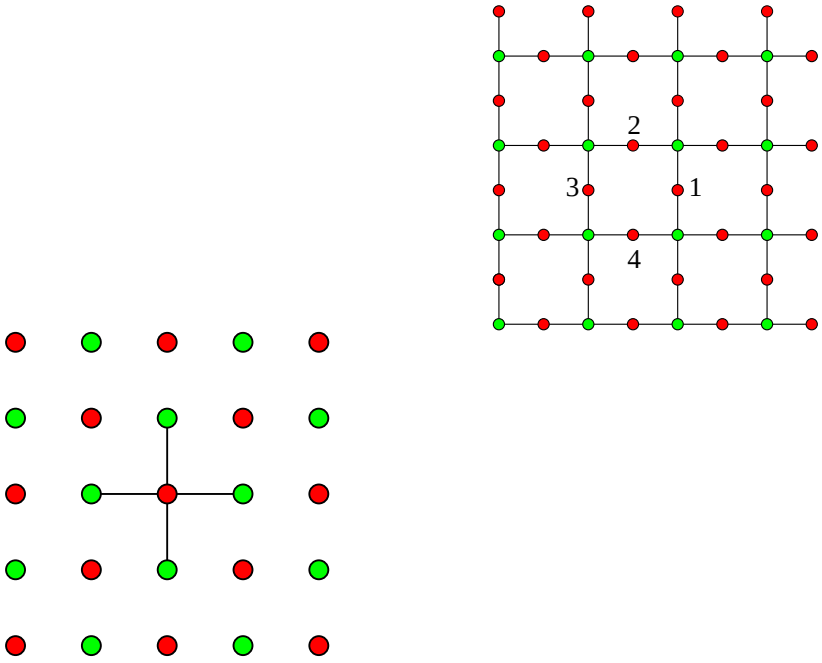

Fig. 2:

Aside: The serious student of the Hubbard model would do well to compute $E(k_x, k_y)$ for a honeycomb geometry. This is useful 'technical' practice, as dealing with axes which are not parallel to $\hat{x}$ and $\hat{y}$ requires some care. It is also of course very interesting physically towards the understanding of graphene. Just as the dispersion relation of the square lattice has interesting properties like Fermi nesting,.
This same result can of course be obtained from the procedure we have outlined earlier. Going to momentum space results in a 3x3 matrix

$$\begin{pmatrix} 0 & -t\left(1+e^{ik_x}\right) & -t\left(1+e^{ik_y}\right) \\ -t\left(1+e^{-ik_x}\right) & 0 & 0 \\ -t\left(1+e^{-ik_y}\right) & 0 & 0 \end{pmatrix} \tag{20}$$

one of whose energy bands is $E_{\mathbf{k}} = 0$.

Localization by Disorder

Examining Eqs. 6 and 6, it is clear that disorder in the hoppings or chemical potentials (making the energy for a fermion to occupy a particular location site-dependent) can be simply incorporated by changing the matrix elements. The transformation Eq. 7 no longer diagonalizes the Hamiltonian, as translation invariance is broken. However the diagonalization can still be accomplished numerically.

A very interesting phenomenon occurs. While the plane wave eigenstates in the absence of randomness extend throughout the lattice, the eigenstates in the presence of disorder can be 'localized', meaning that the components of the eigenstate are significant only on a fraction of the sites and exponentially small elsewhere. In the generic situation the eigenstates near the

center of the DOS are delocalized, and those the edges (high and low energies) are localized, with a 'mobility edge' separating the two cases.

Here one can return to the analogy with classical systems, and a beautiful discussion of Maradudin which describes localization about a single defect mass in a 1D mass-spring chain [9].

There is a lot to unpack in the comments above, and indeed there was an effort over more than a decade to understand the nature of localization in two dimensions. But the main message for us here is that many aspects of this deep and beautiful chapter of condensed matter physics conform to the title of this chapter: From a computational perspective they boil down to the very familiar and simple question of diagonalizing a matrix!

4 The Hatano-Nelson model

A recently emerging area of interest concerns non-Hermitian Hamiltonians [10–12]. The simple methods we have introduced give us a foothold into this field as well. For concreteness, let's consider the 'Hatano-Nelson Hamiltonian' in one dimension:

$$\hat{\mathcal{H}} = -t \sum_{l=1}^{L} (\, e^{h} \, \hat{c}_{l+1}^{\dagger} \hat{c}_{l} + e^{-h} \, \hat{c}_{l}^{\dagger} \hat{c}_{l+1} \,) + \sum_{l} \mu_{l} \, \hat{c}_{l}^{\dagger} \hat{c}_{l} \ . \tag{21}$$

which is obtained from the Hubbard model of Eq. 6 by introducing a hopping which is different for fermions moving to the left and to the right. The parameter h controls the degree of anisotropy in the hopping, and μ_l are random site energies. Periodic boundary conditions connect sites 1 and L.

In the case where there is no disorder, $\mu_l = 0$, we can try the same canonical transformation as Eq. 7, which leads to eigenvalues then have the form,

$$E(k) = -t(e^{-h-ik} + e^{h+ik}) = -2t\cosh(h)\cos(k) - 2t\sinh(h)\sin(k) \ . \tag{22}$$

As k varies from 0 to 2π (in steps of $\frac{1}{L}$) this describes an ellipse centered at the origin of the complex plane. The length of the ellipse along the real axis is $4t \cosh(h)$ and along the imaginary axis, $4t \sinh(h)$. The periodic boundary conditions are crucial. Without them one can do a 'gauge transformation', or in more elementary language a redefinition of the eigenvectors, which makes h disappear from the problem: $\tilde{v}_l = e^{-hl} v_l$. Then the matrix is Hermitian, with all real eigenvalues.

As remarked earlier, in the presence of disorder the transformation of Eq. 7 no longer works. Instead one simply diagonalizes the matrix,

$$H = \begin{pmatrix} \mu_1 & -t\,e^{h} & 0 & 0 & 0 & \cdots & -t\,e^{-h} \\ -t\,e^{-h} & \mu_2 & -t\,e^{h} & 0 & 0 & \cdots & 0 \\ 0 & -t\,e^{-h} & \mu_3 & -t\,e^{h} & 0 & \cdots & 0 \\ \vdots & \vdots & \vdots & & & \vdots & \ddots \\ -t\,e^{h} & 0 & 0 & 0 & 0 & -t\,e^{-h} & \mu_L \end{pmatrix} \tag{23}$$

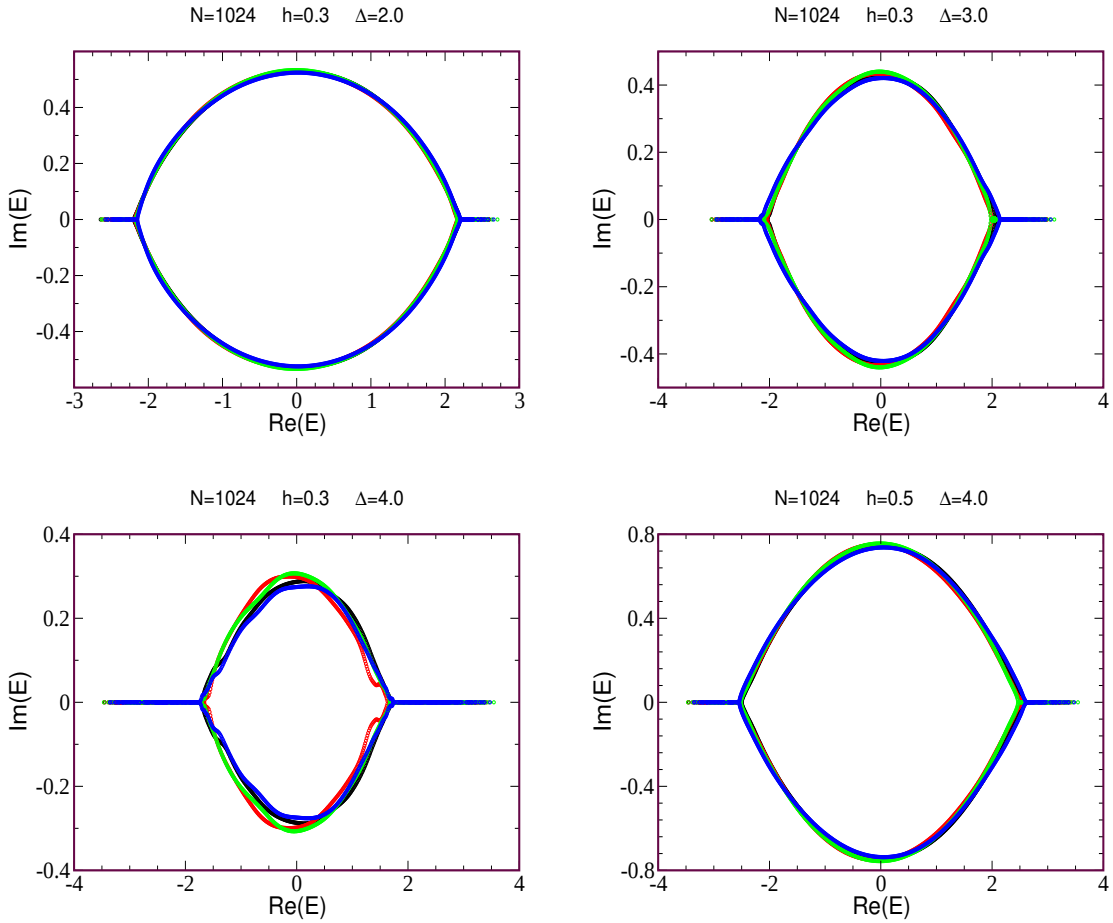

Fig. 3: *Left: Eigenvalues of the Hatano-Nelson Hamiltonian for an $N = 1024$ site chain. The random chemical potentials are chosen from a box distribution $-\Delta < \mu_l < +\Delta$. Four disorder realizations are shown in each figure. As the disorder Δ increases at fixed h the real 'wings' become longer. As h increases at fixed Δ the imaginary part of the eigenvalues grows.*

When disorder is present, the original elliptical distribution in the complex plane develops 'wings' extending out along the real axis. See Fig. 3. The eigenvectors associated with the real eigenvalues on the wings are localized, and those on the wings are real. The plausibility argument for this assertion is that even with periodic boundary conditions one can in fact accumulate the h factors on any desired link (or set of links) through the gauge transformation note above. For a localized eigenvector one can move all the h factors to a lattice location where the wave function is arbitrarily (exponentially) small. So those eigenvectors are governed by a piece of H which can be made Hermitian in the only part of the lattice that matters to them. They will have real eigenvalues. This doesn't work for extended eigenvectors, so they have complex eigenvalues.

The numerical result of Fig. 3 reveal some interesting general features of computational work on Hubbard models (and even more generally). Except for $h = 0.3, \Delta = 4.0$ $N = 1024$ is large enough that the results are 'self-averaging': Different disorder realizations largely coin-

cide. However, when h is small and the disorder is large enough, one begins to see significant variation from realization to realization. It is also the case that locating the position where the real eigenvalues transition to complex ones would likely require careful finite size analysis. The $N = 1024$ dimensional matrices can be diagonalized in about one half of a minute using the LAPACK routine *dgeevx*. Diagonalization scales as N^3 so $N = 4096$ would only take about a half-hour.

5 Perfect Quantum state transfer

One of the most familiar and prominent aspects of quantum mechanics is the uncertainty principle. The uncertainty in our knowledge of the position and momentum of a quantum mechanical particle must obey $\Delta x \Delta p \geq \hbar/2$. Moreover, in many cases we expect uncertainties in position to grow in time ('spreading of the wav packet'). Consider a particle moving in $d = 1$ with no potential $V(x) = 0$. A crude argument is that the This reasoning uggests Δx should grow linearly in time, but, actually, the correct result is that $\Delta x \sim \sqrt{t}$ as can be seen by explicitly solving the free particle Schroedinger equation or else simply by noting its similarity to the classical diffusion equation.

It is therefore remarkable that we can construct Hubbard models which exhibit 'perfect quantum state transfer' (QST). That is, a wavefunction perfectly localized at one end of a $d = 1$ chain will, at later times, be perfectly localized at the opposite end! Although spreading does occur at intermediate times, the wave function somehow re-coalesces to have zero position uncertainty.

How does this (quantum mechanically) counter-intuitive result occur?
Theoretical demonstration of this approach has been put forward in the case of an N-site one-dimensional (1D) XY-model quantum spin chain [13] ($\hbar = 1$):

$$\hat{H} = \sum_{\langle i,j \rangle}^{N} J_{ij} \left[\hat{\sigma}_i^+ \hat{\sigma}_j^- + \hat{\sigma}_i^- \hat{\sigma}_j^+ \right], \tag{24}$$

where $\hat{\sigma}_i^+$ ($\hat{\sigma}_i^-$) is the raising (lowering) operator for qubit Q_i, and the nearest-neighbor (NN) coupling between a pair of qubits is given by J_{ij}. The key observation is that provided the couplings are chosen to satisfy $J_{n,n+1} = J\sqrt{n(N-n)}$ for $n = 1, \ldots, N-1$, the Hamiltonian (24) in the single-excitation subspace is equivalent to that of a large $(N-1)/2$-spin $\vec{S}$ under the application of a homogeneous magnetic field, i.e., $\hat{H}/J = \hat{S}_+ + \hat{S}_- = 2\hat{S}_x$, where $\hat{S}_+$ ($\hat{S}_-$) is the raising (lowering) operator of the large spin. This mapping makes it clear how a perfect QST is realized: An initial state consisting of a single excited qubit Q_A, while the remaining qubits are in their lowest states, $|\psi(0)\rangle = |1_A 00 \cdots 00_B\rangle$, corresponds to the maximal projection of the spin along the z-quantization axis in the mapped Hamiltonian. Since the effect of the x-oriented uniform field is to precess the large spin, it is evident that at time $tJ = \pi/2$, the state will have full projection along the $-z$-direction. Translating back to the original Hamiltonian, this state corresponds to the reflection-symmetric state $|\psi(tJ = \pi/2)\rangle = |0_A 00 \cdots 01_B\rangle$. Such a perfect

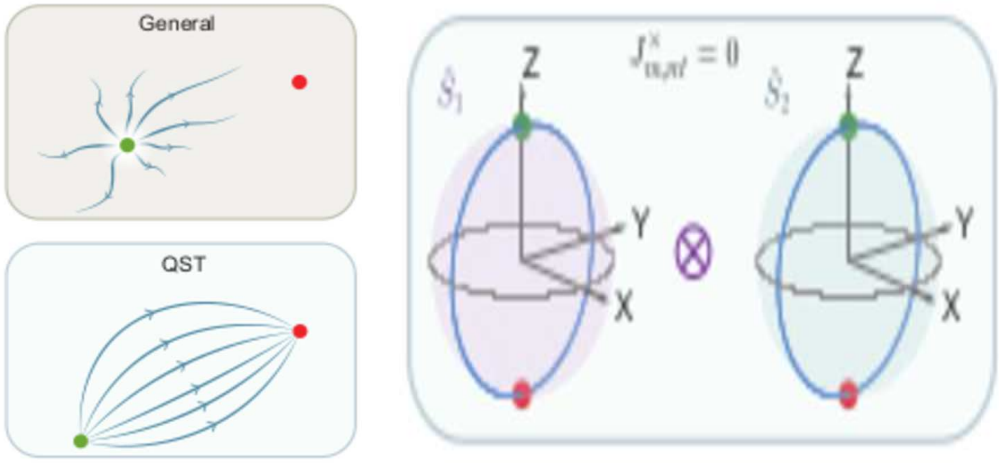

Fig. 4:

QST scheme between opposite qubits Q_A and Q_B in a 1D chain has been previously realized in superconducting quantum circuits featuring four qubits [15].
Generalization of these results to higher dimensions is readily obtained in theory [14]. For example, in a bipartite lattice in D dimensions, the constraints in the inter-qubit nearest-neighbor couplings satisfy a similar expression: $J^{(d)}_{n,n+1} = J\sqrt{n(N_d - n)}$, for $n = 1, \ldots, N_d - 1$ and $d = 1, \ldots, D$. The corresponding mapped large-spin Hamiltonian, $\hat{H}_D/J = 2\hat{S}_{1,x} + 2\hat{S}_{2,x} + \ldots + 2\hat{S}_{D,x}$, describes a collection of D large $(N_d - 1)/2$ spins, each independently precessing around its x-axis at the same rate, thereby guaranteeing perfect QST at time $tJ = \pi/2$.

6 The Strong Coupling Limit

Make PHS from the get-go

The preceding section concerned the noninteracting limit, $U = 0$. Let's consider her what happens in the opposite extreme of no hopping, $t = 0$. The Hubbard model then
We can get a first insight into the Hubbard model by considering just a single site. Alternately phrased, we can set $t = 0$ in the Hamiltonian, in which case we have a collection of independent sites. The one site model is easily solved. We have four possibilities corresponding to the site being empty, having a single electron (either spin up or spin down) or being doubly occupied. Each of the states $|0\rangle, |\uparrow\rangle, |\downarrow\rangle, |\uparrow\downarrow\rangle$ is an eigenstate of H with eigenvalues $0, -\mu, -\mu, U - 2\mu$ respectively. The partition function is

$$Z = \sum_\alpha \langle\alpha|e^{-\beta H}|\alpha\rangle = 1 + 2e^{\beta\mu} + e^{2\beta\mu - \beta U},$$

and the energy is,

$$E = \langle H + \mu n\rangle = Z^{-1} \sum_\alpha \langle\alpha|He^{-\beta H}|\alpha\rangle = (1 + 2e^{\beta\mu} + e^{2\beta\mu-\beta U})^{-1}\, U\, e^{2\beta\mu-\beta U}.$$

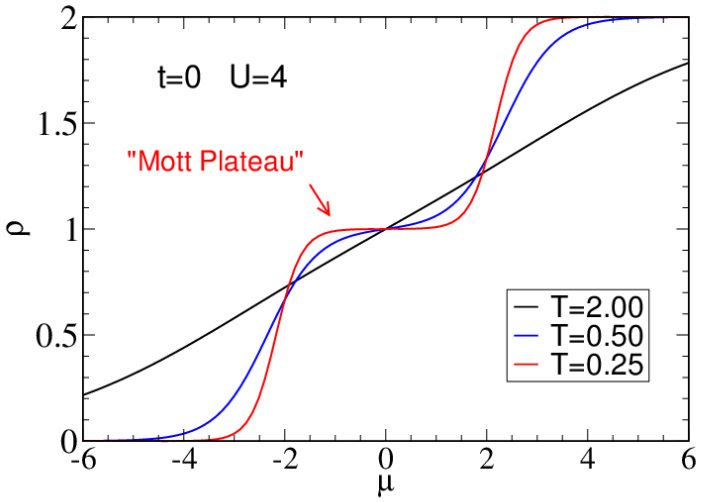

Fig. 5: *Density ρ as a function of chemical potential μ for the single site ($t = 0$) HH. As the temperature decreases, a "Mott Plateau" develops: Increasing μ initially adds a fermion to the site, but ρ gets frozen at $\rho = 1$. The chemical potential must jump by $\Delta\mu = U$ to add a second fermion. The compressibility $\kappa = \partial\rho/\partial\mu = 0$ in the Mott gap.*

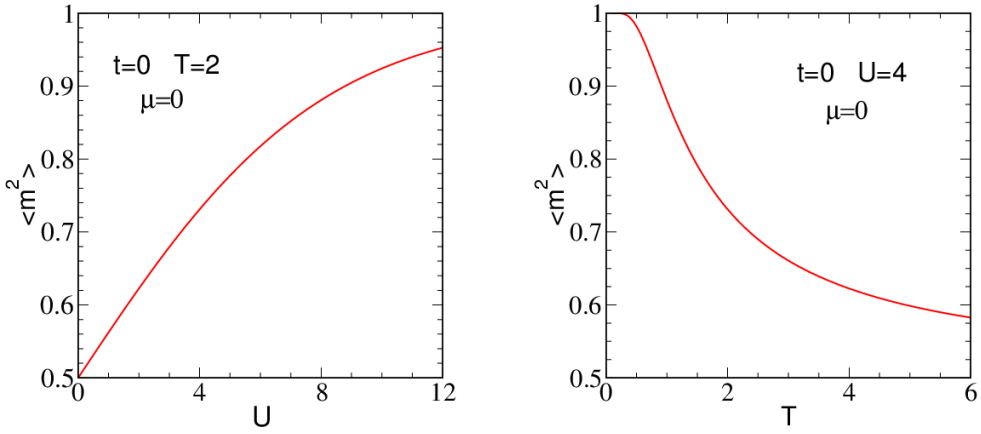

Fig. 6: *Left: The local moment $\langle m^2 \rangle$ as a function of U at fixed temperature $T = 2$. Right: The local moment $\langle m^2 \rangle$ as a function of T at fixed temperature $U = 4$. Local moments develop as either T is reduced or U is increased. Chemical potential $\mu = 0$ in both panels, so the site is half-filled.*

Exercise 12: Show that the occupation is given by,

$$\rho = \langle n \rangle \quad = 2(1 + 2e^{\beta\mu} + e^{2\beta\mu - \beta U})^{-1}(e^{\beta\mu} + e^{2\beta\mu - \beta U})$$

Plot ρ vs. μ for $U = 4$ and $T = 2$. Plot ρ vs. μ for $U = 4$ and $T = 0.5$.

The plots of ρ versus μ you made in Exercise 12 exhibit some of the fundamental physics of

the Hubbard model, namely the "Mott insulating gap". This will be discussed in more detail in Section IX, but for now, consider the following: at $T = 0$ the chemical potential μ has the property that $\mu = \partial E/\partial\rho$. In words, μ tells you how much the energy changes when you change the density of the system. If you have a noninteracting system described by a set of energy levels, and you have filled the levels up to some 'Fermi energy' E_F the cost to add a particle is the next energy level just above the last level you filled, that is, $\mu = E_F$.
If you reach a gap, a region of energy where there are no further levels to be filled, then μ has to take a jump from the energy at the top of the band which has just been filled to the energy at the bottom of the next band. Thus a jump in μ reflects the existence of a gap (and hence that your system is insulating). It turns out that even when interactions are turned on, and you cannot describe the system in terms of a bunch of energy levels, a jump in μ still indicates the existence of a gapped, insulating phase.
In Exercise 12 you found that at low temperature ($T = 0.5$) μ jumps suddenly to a higher value when the filling crosses through $\rho = 1$. This is the most simple indication of a 'Mott' insulating phase in the half-filled Hubbard model.
In Exercise 12 you should have found that you are at half-filling $\rho = 1$ when $\mu = U/2$. Because half-filling is so often studied, it is convenient to write the Hubbard Hamiltonian as,

$$H = -t \sum_{\langle \mathbf{j},\mathbf{l}\rangle\sigma} c^\dagger_{\mathbf{j}\sigma} c_{\mathbf{l}\sigma} + U \sum_{\mathbf{j}} (n_{\mathbf{j}\uparrow} - \frac{1}{2})(n_{\mathbf{j}\downarrow} - \frac{1}{2}) - \mu \sum_{\mathbf{j}} (n_{\mathbf{j}\uparrow} + n_{\mathbf{j}\downarrow})$$

This just corresponds to a shift in the chemical potential μ by $U/2$. When this is done, half-filling conveniently occurs always at $\mu = 0$ for any value of t, T, U. To emphasize, the properties of this 'new' model are identical to the old one, if one compares them at the same density. It's just that the chemical potentials used to get those densities are offset.

Exercise 14: Write expressions for Z, E and ρ with this new convention for the interaction term in the Hubbard model. You should notice that they are a bit more symmetric looking at $\mu = 0$.

It is also instructive to look at the Green's function for a single site, that is, the $t = 0$ Hubbard model. We have previously written down the Hilbert space for this problem and obtained the partition function and various equal time quantities. Now consider the calculation of

$$G_\uparrow(\tau) = \langle c_\uparrow(\tau) c^\dagger_\uparrow(0)\rangle.$$

Only the states $|\,0\,0\,\rangle$ and $|\,0\,1\,\rangle$ contribute to the expectation value since the creation operator for up electrons needs to see an empty up state. We can easily compute the action of the sequence of operators on $|\,0\,0\,\rangle$:

$$\begin{aligned} c_\uparrow(\tau) c^\dagger_\uparrow(0)\ |\,0\,0\,\rangle &= e^{H\tau} c_\uparrow(0) e^{-H\tau} c^\dagger_\uparrow(0)\ |\,0\,0\,\rangle = e^{H\tau} c_\uparrow(0) e^{-H\tau}\ |\,1\,0\,\rangle \\ &= e^{H\tau} c_\uparrow(0) e^{+U\tau/4}\ |\,1\,0\,\rangle = e^{H\tau} e^{+U\tau/4}\ |\,0\,0\,\rangle = e^{+U\tau/2}\ |\,0\,0\,\rangle \end{aligned}$$

and similarly for $|\,0\,1\,\rangle$.

Exercise 46: Complete the calculation begun above to show that,

$$G_\uparrow(\tau) = \frac{e^{+\beta U/4} e^{-\tau U/2} + e^{-\beta U/4} e^{\tau U/2}}{2\, e^{\beta U/4} + 2\, e^{-\beta U/4}}.$$

Exercise 47: The Green's function is related to the spectral density $A(\omega)$ by the relation,

$$G(\tau) = \int_{-\infty}^{+\infty} A(\omega) \frac{e^{-\omega\tau}}{e^{-\beta\omega}+1}\, d\omega.$$

Show that if you plug in

$$A(\omega) = \frac{1}{2}\, (\, \delta(\omega - U/2) + \delta(\omega + U/2)\,)$$

and do the integral you get precisely the $G(\tau)$ we computed.

This is one way (there are others) to show that the spectral function in Hubbard-1 consists of two delta function peaks separated by U (the Mott gap).

7 Particle-Hole Transformations

Before introducing the main results of this work, it is useful to review the well-known (partial) particle-hole transformation $c_{i\downarrow} \rightarrow (-1)^{i_x+i_y}\, c^\dagger_{i\downarrow}$ which links the descriptions of the properties of the attractive and repulsive cases. Here $(-1)^{i_x+i_y}$ indicates opposite phases on the two sublattices of the (bipartite) square lattice. Under this transformation, the kinetic energy remains unchanged. The down spin density $n_{i\downarrow} \leftrightarrow 1 - n_{i\downarrow}$ and, as a consequence the sign of U is reversed, mapping attraction to repulsion and vice-versa. The roles of charge and spin operators are interchanged $n_{i\uparrow} + n_{i\downarrow} \leftrightarrow n_{i\uparrow} - n_{i\downarrow}$, so that chemical potential μ and Zeeman B_z terms map into one another (to within an irrelevant energy shift) and correlations of the Z component of spin map onto density correlations. Finally, the XY spin operators map onto s-wave pairing $c^\dagger_{i\uparrow} c_{i\downarrow} \leftrightarrow c^\dagger_{i\uparrow} c^\dagger_{i\downarrow}$.

With those mappings in place, the connections between the attractive and repulsive Hubbard models become clear. The fact that the square lattice repulsive Hubbard model has degenerate Z and XY spin order in its ground state and half-filling immediately implies the degenerate CDW and SC patterns in the attractive case. Likewise, the fact that a Zeeman field B_z causes AF Heisenberg spins to 'lie down' and order in the XY plane perpendicular to the field is then connected to the preference for SC correlations over CDW ones in the attractive Hubbard model for μ nonzero. We will now show how an alternate canonical transformation lends similar insight into exotic superconductivity.

Attractive σ_z-Hubbard model.— We then apply the unitary transformation, $c_{i\downarrow} \rightarrow \mathrm{sgn}(i) c_{i\downarrow}$, to

the attractive Hubbard model, resulting in the σ_z-Hubbard model defined by the Hamiltonian,

$$\mathcal{H}_{\sigma_z} = -t \sum_{\langle ij \rangle} \sum_{\alpha\beta} c^{\dagger}_{i\alpha} \sigma_z^{\alpha\beta} c_{j\beta} - \mu \sum_{i,\alpha} n_{i\alpha} \\ +U \sum_i (n_{i\uparrow} - \frac{1}{2})(n_{i\downarrow} - \frac{1}{2}) \tag{25}$$

where σ_z represents the Z-component of the Pauli matrix, resulting in opposite signs in the hopping amplitudes for the spin-up and spin-down subsystems.

The phase diagram of the attractive Hubbard model can be transformed back to derive that of the attractive σ_z-Hubbard model. It is observed that while the CDW remains unaffected, the s-wave SC phase is altered. Specifically, the on-site pairing transforms back as $\Delta_j = c_{j\downarrow} c_{j\uparrow} \rightarrow \Delta_j = \text{sgn}(j) c_{j\downarrow} c_{j\uparrow}$. Therefore, the pairing remains on-site but with an alternating sign, indicating that the system displays s-wave PDW superconductivity. The pairing function can be written as $\Delta^{\dagger} = \frac{1}{\sqrt{N}} \sum_j (-1)^{j_x + j_y} c^{\dagger}_j c^{\dagger}_j = \frac{1}{\sqrt{N}} \sum_{\mathbf{k}} c^{\dagger}_{\mathbf{k}} c^{\dagger}_{-\mathbf{k}+\mathbf{K}_0}$ with $\mathbf{K}_0 = (\pm\pi, \pm\pi)$. Therefore a PDW state, in which an electron at momentum $\mathbf{k}$ pairs up with another at momentum $-\mathbf{k} + \mathbf{K}_0$, resulting in a Cooper pair carrying net momentum $\mathbf{K}_0$, must rigorously be the low temperature phase of the attractive σ_z-Hubbard model.

References

[1] Patrik Fazekas: *Lecture Notes on Electron Correlation and Magnetism* (World Scientific, Singapore, 1999)

[2] T. Esslinger, Annu. Rev. Condens. Matter Phys. 1, 129 (2010).

[3] L. Tarruell and L. Sanchez-Palencia, Comptes Rendus Physique 19, 365 (2018).

[4] J. Zaanen and O. Gunnarsson, Physical Review B 40, 7391, (1989).

[5] J.P.F. LeBlanc *etal*, Phys. Rev. X 5, 041041 (2015).

[6] S.R. White and D.J. Scalapino, Physical Review Letters 91, 136403, (2003).

[7] K. ChŃg, J. Carrasquilla, R.G. Melko, and E. Khatami, Physical Review X 7, 031038, (2017).

[8] D.P. Arovas, E. Berg, S.A. Kivelson, and S. Raghu, Annual review of condensed matter physics 13, 239 (2022).

[9] A.A. Maradudin, P. Mazur, E.W. Montroll, and G.H. Weiss, Reviews of Modern Physics 30, 175, (1958).

[10] J. Feinberg and A. Zee, Nucl. Phys. B504, 579 (1997).

[11] C.M. Bender, Reports on Progress in Physics 70, 947 (2007).

[12] Y. Ashida, Z. Gong, and M. Ueda, Advances in Physics 69, 249 (2020).

[13] M. Christandl, N. Datta, A. Ekert, and A.J. Landahl, Phys. Rev. Lett. 92, 187902 (2004).

[14] A. Kay, International Journal of Quantum Information 08, 641 (2010).

[15] X. Li, Y. Ma, J. Han, T. Chen, Y. Xu, W. Cai, H. Wang, Y.P. Song, Z-Y.. Xue, Z-q. Yin, and L. Sun, Phys. Rev. Appl. 10, 054009 (2018).